Int J Environ Res (2025) 19:31
https://doi.org/10.1007/s41742-024-00698-z

RESEARCH PAPER

Transport of Nanoplastics in Saturated Zeolite: Effects of Flow Rate and Hydro-Chemical Conditions

Taotao Lu[1,3] · Xue Bai[1] · Hao Peng[2,3] · Zhu Xu[4] · Geng Niu[3] · Sven Frei[5]

Received: 13 June 2024 / Revised: 16 October 2024 / Accepted: 2 November 2024

Abstract

Aluminosilicates are commonly present in natural soils, contributing to their texture and composition. The fate and transport of nanoplastics within natural sediments containing aluminosilicates have not been comprehensively studied yet. To investigate the interactions between nanoplastics and sediments, polystyrene nanoplastics (PS-NPs) were injected into columns filled with zeolite under the condition of different flow rates, pH values, and ionic strengths (IS). Results show that zeolite inhibited polystyrene nanoplastics (PS-NPs) transport to different extents under different conditions. The limitation of PS-NPs transport was mainly governed by (1) the PS-NPs–zeolite interaction energy obtained via the Derjaguin–Landau–Verwey–Overbeek calculation, (2) the amphoteric sites on zeolite surface (they will possess positive charges attracting negative PS-NPs when $pH < pH_{pzc}$), and (3) surface roughness leading to physical straining phenomena. In addition, the flow rate of pore water played an essential role during the PS-NPs transport. The retention of PS-NPs decreased at higher flow rates, likely due to a reduction in particle-collector contact efficiency. This study uncovers the migration mechanism of PS-NPs within zeolite, providing insights into the behavior of nanoparticles in natural porous media.

Highlights

- **Zeolite significantly alters PS-NPs flow under diverse conditions.**
- **Amphoteric sites on zeolite surface edges affect PS-NPs transport.**
- **Increased flow rates boost PS-NPs mobility effectively.**
- **Varying ionic strength impacts PS-NPs retention notably.**
- **Different cation types crucially influence PS-NPs transport.**

Taotao Lu and Xue Bai contributed equally.

✉ Hao Peng
penghao@cug.edu.cn

[1] College of Hydraulic Science and Engineering, Yangzhou University, Yangzhou 225009, China

[2] College of Environment and Civil Engineering, Chengdu University of Technology, Chengdu 610059, China

[3] Wuhan Zondy W&R Environmental Technology Co., Ltd, Wuhan 430078, China

[4] Yangzhou Haitong Electronic Co. Ltd, Yangzhou 225001, China

[5] Aquatic Ecology and Water Quality Management Group, Department of Environmental Science, Wageningen University Research Centre, Wageningen 6700 AA, The Netherlands

Published online: 18 November 2024

Keywords Polystyrene nanoplastics · Transport · Zeolite · Amphoteric site

Introduction

With economic development, polymers have been widely utilized in daily life products, such as personal care products, electronic devices, and packing materials. The expected total amount of produced plastics will exceed 33 billion tons by 2050 (Sharma et al. 2020). Due to ineffective recycling policies, plastics can be found in high amounts in natural systems such as lakes, oceans, rivers, streams, and terrestrial systems (Kumar et al. 2021). Larger plastic debris can be degraded and fragmented via weathering, photo-oxidation, and biodegradation, into nanoplastics (fragments less than 100 nm) (Andrady et al. 2022; Wang et al. 2019, 2022; Yu et al. 2024). Research has shown that nanoplastics (NPs) can penetrate cell membranes, raising concerns about their potential harmful effects, which have attracted significant global attention (Qiana et al. 2024). The associated health risks are extensive, encompassing oxidative stress, cytotoxicity, metabolic alterations, immune system disruption, translocation to distant organs, neurotoxicity, reproductive toxicity, and carcinogenicity (Rahman et al. 2021; Zhang et al. 2024). In terrestrial environments, NPs are known to negatively affect plant growth by adhering to plant roots, altering soil properties, and disrupting microbial communities (Qu et al. 2023). Furthermore, human exposure to microplastics and NPs can occur via ingestion, inhalation, and dermal contact, potentially exacerbating inflammatory responses and increasing the risk of non-communicable diseases (Shen et al. 2019). As high abundances of NPs have been found in various soil and groundwater systems (Castan et al. 2021), it is important to understand the mechanisms controlling the fate and transport of NPs in subsurface environments (Lai et al. 2022; Ma et al. 2023; Yu and Flury 2021).

Compared to larger plastic debris, the distinctive properties of NPs—such as their higher surface-to-volume ratio and enhanced ability to remain suspended in water—significantly influence their transport through soil and groundwater aquifers (Liu et al. 2021; Lu et al. 2021b). The increased surface area of NPs facilitates greater interaction with water molecules, dissolved substances, and particulates, enhancing their stability and suspension in water columns (Lai et al. 2022). This stability increases the residence time of NPs in the water column, thereby enhancing the potential for biological uptake and subsequent incorporation into the food chain. Moreover, their ability to remain suspended in water for extended periods contributes to their enhanced dispersion and broader transport ranges. These characteristics promote a more uniform distribution of NPs in aquatic environments, potentially increasing exposure to aquatic organisms (Chen et al. 2024; Hu et al. 2019). To date, most research on NP transport has been conducted using pure quartz sands as a model system for porous media. In-depth studies have been carried out through adsorption and column experiments (Liu et al. 2024; Zhang et al. 2023a, b). However, these oversimplified settings often fail to represent the complex conditions in natural subsurface environments (Yu and Flury 2021). Recently, an increasing number of studies have begun to investigate the mechanisms controlling the transport of nanoplastics under more realistic experimental conditions. The effect of different alumino-silicate minerals on NPs transport within saturated porous media was investigated by Lu et al. (2021a). NP retention in porous media containing illite or kaolinite was significantly higher than in pure quartz sand, likely due to the abundance of amphoteric sites on the surfaces of the aluminosilicate minerals (Shu et al. 2024).These sites could favor polystyrene nanoplastics (PS-NPs) deposition (Lu et al. 2021a). Increased mobility of PS-NPs was observed at higher pH levels; for instance, at pH 9, the edge sites of alumino-silicate minerals become less positively charged, which reduces the deposition rate of the negatively charged PS-NPs. These results are very relevant for natural porous media environments as natural soils and aquifers usually contain alumino-silicate minerals affecting the physicochemical properties of porous media significantly. Different alumino-silicate minerals show different extents in the isomorphic substitution that happened in the mineral crystals and different abilities of protonation/deprotonation (Fan et al. 2024; Liang et al. 2023; Lin et al. 2023). As a result, different alumino-silicate minerals may exert different influences on the NPs transport. Zeolite, a naturally occurring alumino-silicate mineral, is ubiquitous in the subsurface (Motsi et al. 2009). However, the effects of zeolite on NPs transport are still unclear.

The primary objective of this research is to elucidate the effects of zeolite on the transport and retention behavior of polystyrene nanoplastics (PS-NPs) under varying solution chemistries and flow rates in water-saturated conditions.The study is organized around several specific objectives: (1) to investigate the impact of zeolite on the mobility of polystyrene nanoplastics (PS-NPs) in water-saturated environments; (2) to analyze the transport patterns of PS-NPs through a series of column experiments; (3) to examine how variations in solution chemistry—specifically pH, cation species, and ionic strength—affect the transport of PS-NPs; (4) to assess the influence of pore water velocities on the mobility

of PS-NPs in a zeolite-packed system; and (5) to apply the Derjaguin–Landau–Verwey–Overbeek (DLVO) theory to quantify the interaction energies between nanoplastics and minerals, helping to interpret the retention patterns observed in the experiments.

Materials and Methods

Materials

Carboxylate coated PS-NPs were purchased from Huge Biotechnology Co., Ltd. (Shanghai, China). The average diameter of the PS-NPs was approximately 100 nm, as confirmed by the TEM images presented in Figure S1. The PS-NPs stock solution was diluted using deionized water to prepare PS-NPs suspension (~ 10 mg/L) used in the experiments. Furthermore, the pH values of the PS-NPs suspension (5.9–9) were adjusted using 0.1 M HCl and NaOH. The ionic strength (1–10 mM) was adjusted using 0.1 M NaCl. At last, various monovalent and divalent cations (e.g., NaCl, KCl, CsCl, $MgCl_2$, $CaCl_2$, and $BaCl_2$), which were analytical reagents obtained from Shanghai Macklin Reagent Co. Ltd., Shanghai, China, were used to investigate the impact of different types of cations. A zetasizer (Nano ZS90) was used to measure zeta potentials and hydrodynamic diameters (Malvern Instrument, UK). The specific method can be found as part of the Supplementary Material (Sze et al. 2003).

Zeolite with a particle size of 60–80 mesh was purchased from a Mineral Trading Company located in Huangshi, China. The pore size desnity of the zeolites ranges from 0.10 to 0.35 cm^3/g (Sowunmi et al. 2018; Szala et al. 2015). The average grain size was ~ 0.21 mm, with a rough surface (SEM images were provided in Figure S2). Based on Brunauer–Emmett–Teller (BET) measurements, the average surface area of the zeolite minerals was 29.1 m^2/g. According to the method provided by Qi et al. (2014), the zeolite was cleaned to remove impurities before being used as part of the column experiments. X-ray Diffraction (XRD) and X-ray Fluorescence (XRF) were applied to the cleaned zeolite (see Figure S3). The XRD result showed that the zeolite mainly consisted of Na/Ca clinoptilolite, and the XRF result suggested that zeolite primarily contained 68.6% SiO_2, 14.7% Al_2O_3, 6.9% CaO, 3.7% Fe_2O_3, 3.6% K_2O and 1.2% MgO, which is in line with EDX results.

Column Experiments

As shown in Figure S4, a 1.6 cm inner diameter, 20 cm long borosilicate glass column was utilized during the column experiments (Shanghai Suke Industrial Co., Ltd.). Stainless steel screens were positioned at both ends of the column. The method used for packing the zeolite column was based on our previous study to ensure a uniform distribution (Lu et al. 2017). Approximatley 17 g of zeolite was filled into the column having an average length of 6.0 ± 0.1 cm. During the experiment, a TYD02 syringe pump (Lead Fluid Technology Co., China) was utilized to inject the prepared PS-NPs solution into the column. Before the PS-NPs solution was injected, the packed columns were saturated with 30 mL

Table 1 Experimental protocols of column tests

Column no	Column properties		Input characteristics						
	Porous media	Porosity (−)	Background solution	Flow rate (mL/h)	pH	PS-NPs conc. (mg/L)	ζ-Potential (mV)	Z_{ave}[a] (nm)	d_p/d_c[b]
1	Zeolite	0.361	1 mM NaCl	0.2	5.9	8.7	− 44.6 ± 0.4	100.7 ± 1.6	0.000480
2	Zeolite	0.359	1 mM NaCl	0.4	5.9	8.9	− 44.6 ± 0.4	100.7 ± 1.6	0.000480
3	Zeolite	0.352	1 mM NaCl	0.6	5.9	8.9	− 44.6 ± 0.4	100.7 ± 1.6	0.000480
4	Zeolite	0.367	5 mM NaCl	0.4	5.9	9.4	− 41.9 ± 1.5	100.6 ± 1.4	0.000479
5	Zeolite	0.355	10 mM NaCl	0.4	5.9	8.1	− 33.7 ± 2.9	98.7 ± 1.5	0.000470
6	Zeolite	0.368	1 mM KCl	0.4	5.9	8.5	− 42.7 ± 0.7	103.9 ± 1.9	0.000495
7	Zeolite	0.366	1 mM CsCl	0.4	5.9	9.9	− 41.4 ± 0.3	101.7 ± 0.7	0.000484
8	Zeolite	0.374	0.5 mM $MgCl_2$	0.4	5.9	8.3	− 27.6 ± 2.1	99.8 ± 1.0	0.000475
9	Zeolite	0.377	0.5 mM $CaCl_2$	0.4	5.9	9.7	− 26.8 ± 1.9	106.5 ± 1.0	0.000507
10	Zeolite	0.388	0.5 mM $BaCl_2$	0.4	5.9	8.5	− 22.5 ± 1.9	112.9 ± 0.5	0.000538
11	Zeolite	0.368	1 mM NaCl	0.4	7.0	8.8	− 47.9 ± 1.3	99.1 ± 0.7	0.000472
12	Zeolite	0.353	1 mM NaCl	0.4	9.0	8.6	− 52.1 ± 1.5	100.6 ± 0.4	0.000479

Values following the sign (±) indicate the standard deviation obtained from conducting two replicates

[a]The mean value of the hydrodynamic diameter of PS-NPs

[b]The ratio of the average size of aggregated PS-NPs to the average diameter of zeolite can be expressed as d_p/d_c

deionized water at a rate of 1.0 mL/h; after saturation, the zeolite was equilibrated by 180 mL background electrolyte solution under a flow speed of 6.0 mL/h. Then, 100 mL of PS-NPs solution stored in the syringe was introduced into the column via pumping, followed by the background electrolyte solution at the preset flow rate. An automatic fraction sampler (Huxi Instrument BSZ-40, China) was applied to collect the effluent solution from the column's outlet at fixed time intervals of 20 min. The UV absorbance of PS-NPs was measured via a UV–vis spectrophotometer (Metash Instrument, China) at 220 nm. The concentration of PS-NPs was determined using a calibration curve established prior to the experiments (see Figure S5). The column experiments were performed twice to ensure data reliability. In addition, the porosity and dead volume of the column were calculated by inversely fitting the breakthrough curves (BTCs) of KBr, which was used as a conservative tracer (refer to Figure S6). Table 1 outlines the specific protocol for the column experiments. The calculation of energy profiles between particles and collectors was based on the application of the DLVO theory, and the detailed equations for this calculation can be found in the supplementary material.

Results and Discussion

Effects of Flow Rate on the Transport of PS-NPs in Saturated Zeolite

Figure 1 shows a positive correlation between the flow rate of pore water and the mobility of PS-NPs within the zeolite column. At a flow rate of 0.2 mL/h, PS-NP retention was maximized, with $(C/C_0)_{max}$ reaching 63.4% at approximately 10 pore volumes (PV).With increasing flow rate, the mobility of PS-NPs gradually increased. At the highest flow rate of 0.6 mL/h, $(C/C_0)_{max}$ reached 81.2% after approximately 10 pore volumes (PV). Although previous studies have shown that increased flow velocities generally enhance the transport of other nanoparticles (Liang et al. 2013; Sharma et al. 2014), our results also indicate that pore water flow rate is a critical factor influencing the movement of PS-NPs in saturated zeolite. As the flow rate increases, the particle-collector contact efficiency decreases due to the heightened shear forces acting on the particles at higher flow velocities (Braun et al. 2015). This phenomenon may explain why particle mobility is limited at lower flow velocities. Furthermore, increasing pore-scale flow velocities also can lead to a remobilization of deposited PS-NPs in porous media (Sasidharan et al. 2014). The higher the flow rate, the more easily the retained nanoparticles will detach from the surface of zeolite minerals due to the higher hydrodynamic forces acting on the particles (Wang et al. 2016). Similar to the research conducted by Lu et al. (2021a), which showed that more PS-NPs were trapped inside kaolinite, SEM images also suggest that the rough surface of zeolite may retain a greater number of PS-NPs, particularly at lower flow rates.

Effects of Ionic Strength on the Transport of PS-NPs in Saturated Zeolite

Figure 2a illustrates that the breakthrough capability of PS-NPs in the zeolite-packed columns decreased as ionic strength (IS) increased. The $(C/C_0)_{max}$ was found to be 73.7% at an ionic strength of 1 mM, 34.9% at 5 mM, and 6.8% at 10 mM.

The interaction energies between the mineral surface and the PS-NPs played a key role in determining the deposition behavior of the PS-NPs (see Fig. 2b). Compared to 1 and 5 mM NaCl, the calculated interaction energies (e.g., the height of energy barriers (Φ_{max}) and depth of secondary wells (Φ_{sec})) were the lowest for 10 mM NaCl. This suggests that the PS-NPs could readily surpass the energy barrier and adhere to the zeolite surface. Hence, the increasing IS results in a corresponding increase in the PS-NPs deposition.

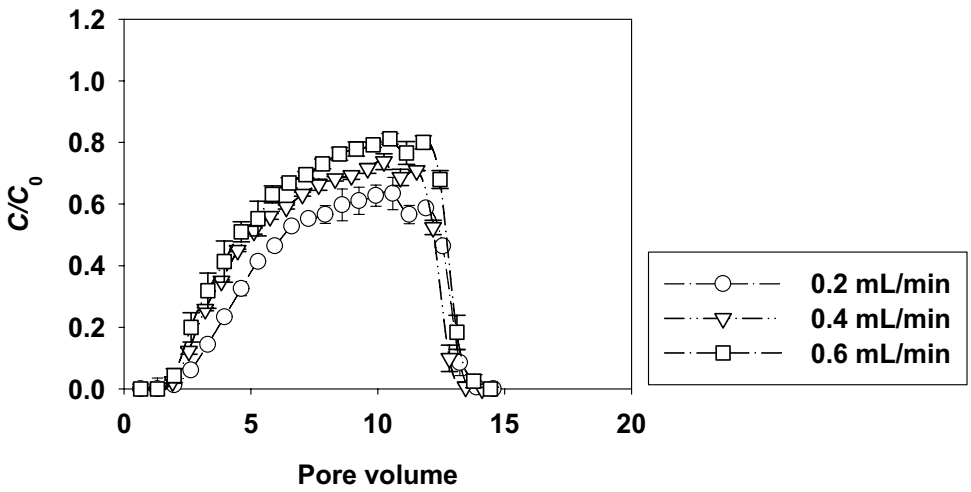

Fig. 1 Effects of flow rate (0.2, 0.4, and 0.6 mL/min) on the transport of PS-NPs in saturated zeolite at a pH of 5.9 and an ionic strength of 1 mM NaCl

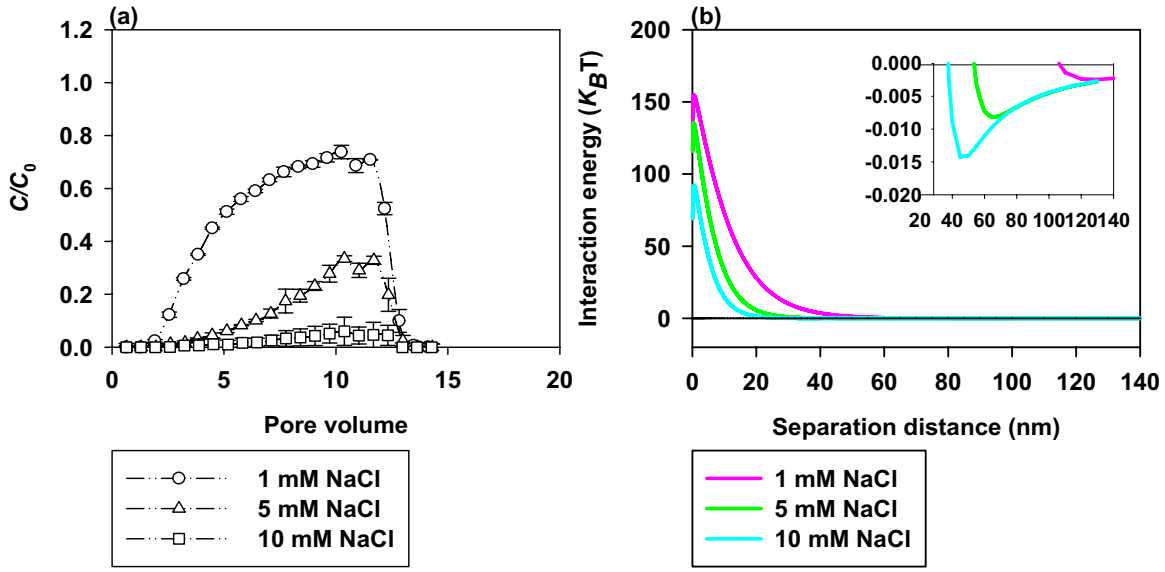

Fig. 2 Effects of ionic strengths (1, 5, and 10 mM NaCl) on the transport of PS-NPs in saturated zeolite at a pH of 5.9 and a flow rate of 0.4 mL/min: **a** breakthrough curves and **b** calculated DLVO interaction energy profiles

Furthermore, the point of zero charge of zeolite was estimated to be around pH 6.5 (Kragovic et al. 2012). The amphoteric sites on the surfaces of zeolite exhibited positive charges at a pH of 5.9, thereby creating more additional sites for PS-NPs deposition. As ionic strength increases, the concentration of ions rises, significantly altering the electrostatic environment around the PS-NPs and zeolite surfaces. At low ionic strengths (e.g., 1 mM NaCl), the electrostatic double layers surrounding the PS-NPs and zeolite are relatively thick, due to the limited number of ions available to disrupt the electric fields generated by surface charges (Miao et al. 2019; Shang et al. 2021). This results in strong electrostatic repulsion between the PS-NPs and zeolite, inhibiting deposition. As the ionic strength increases to 5 mM NaCl, more ions penetrate the double layer, partially neutralizing the surface charges and compressing the electrostatic double layer, which reduces the separation between particles and surfaces and increases the likelihood of interaction. At 10 mM NaCl, the double layer is further compressed, and the charges on both PS-NPs and zeolite are nearly neutralized by the excess ions, drastically reducing repulsion and facilitating deposition (Cai et al. 2018; Wu et al. 2020). These results are consistent with previous findings by Mitzel et al. (2016) and Quevedo and Tufenkji (2012). The PS-NP particles had an average hydrodynamic diameter of approximately 100 nm at 1 mM, 5 mM, and 10 mM NaCl, respectively. Consequently, the dp/dc values presented in Table 1 were significantly lower than the critical threshold of 0.002, indicating that physical straining is unlikely to be a significant mechanism for retention. Under natural conditions, variations in ionic strength could significantly affect the behavior of NPs. In groundwater systems, ionic strength can fluctuate due to geological factors, seasonal variations in rainfall, and anthropogenic activities. The findings from this study are essential for assessing potential ecological impacts and developing strategies to mitigate adverse effects on ecosystems (Fang and Nakagawa 2021; Liu et al. 2024).

Effects of Different Cations on the Transport of PS-NPs in Saturated Zeolite

Results for the column experiments using different cation species are presented in Fig. 3a. In general, the mobility of PS-NPs was observed to decrease in the following order for cations: $Na^+ > K^+ > Cs^+$; $Mg^{2+} > Ca^{2+} > Ba^{2+}$.

Na^+ had a only a small impact on PS-NP mobility, as indicated by a $(C/C_0)_{max}$ of approximately 73.8%. In contrast, the presence of Cs^+ significantly decreased the PS-NPs mobility, with a $(C/C_0)_{max}$ of around 59.7% at 10 PV. For K^+, $(C/C_0)_{max}$ of 67.4% was located between the corresponding ratios observed in the experiments using Na^+ and Cs^+. This observation can be explained using the DLVO theory, which shows that the maximum energy barrier height in Fig. 3b followed a decreasing order: Na^+ (154.5 K_BT) > K^+ (148.2 K_BT) > Cs^+ (134.0 K_BT). When Na^+ is the background cation, the energy barrier is highest, making the deposition process relatively more difficult compared to situations where K^+ or Cs^+ serves as the background cation. Interestingly, the decreasing energy barrier with increasing ionic radius and atomic number aligns with the Hofmeister series. For Cs^+ it was shown that they can act as bridging ions connecting graphene oxide to the grains of porous media Xia et al.

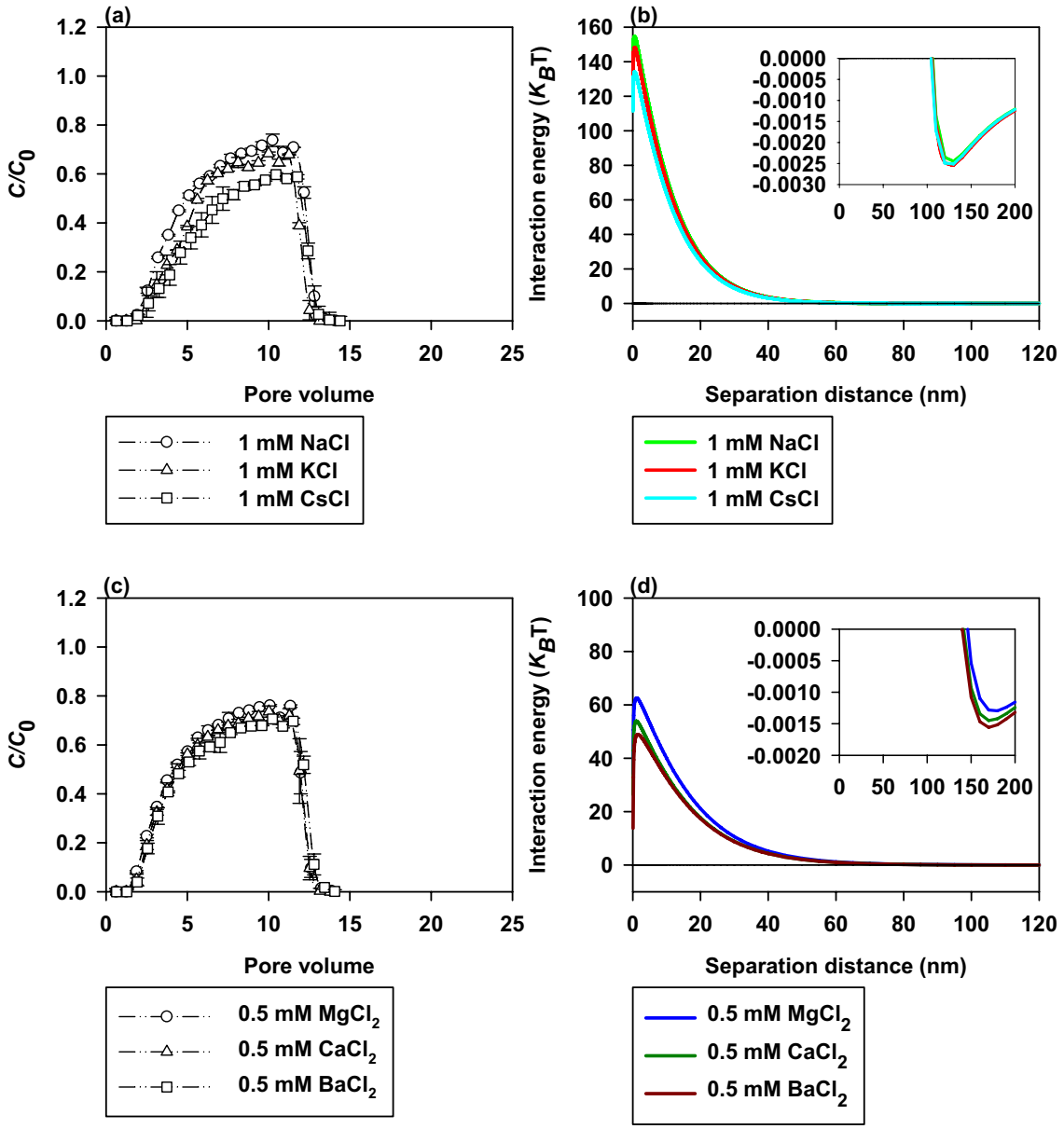

Fig. 3 Effects of cation species (NaCl, KCl, and CsCl; $MgCl_2$, $CaCl_2$, and $BaCl_2$) on the transport of PS-NPs in saturated zeolite at a pH of 5.9 and a flow rate of 0.4 mL/min: **a**, **c** breakthrough curves and **b**, **d** calculated DLVO interaction energy profiles

(2015). However, this bridging function was not observed for Na^+ and K^+. Thus, the increased retention of PS-NPs in the zeolite-packed column in the presence of Cs^+ may be attributed to the bridging effect of Cs^+ ions, which connect the carboxyl groups on the PS-NPs to the zeolite surface. The binding efficiency of PS-NPs to zeolite surfaces, influenced by steric hindrance, is governed by the size of the hydrated cationic radius. This indicates that the accumulation of larger hydrated ions can hinder the ability of PS-NPs to attach to or adsorb onto the zeolite surface (Nightingale Jr, 1959). Table S2 showed that the monovalent cations had different hydrated radii, with Na^+ having the largest, followed by K^+ and Cs^+. This suggests that Cs^+ experienced the least steric hindrance, while Na^+ encountered the greatest steric hindrance. As a result, the column containing Cs^+ resulted in the highest deposition of PS-NPs.

To further validate the Hofmeister effects, additional experiments were conducted to measure how the transport of PS-NPs within zeolite was influenced by divalent cations (see Fig. 3c). Maximum C/C_0 ratios were ~ 76.1% for Mg^{2+} followed by Ca^{2+} with ~ 73.6% and Ba^{2+} with ~ 68.9%. Based on DLVO calculations, the energy profile under the condition of Ba^{2+}showed that Φ_{max} was the lowest and Φ_{sec} was the shallowest (see Fig. 3d). In this context, PS-NPs

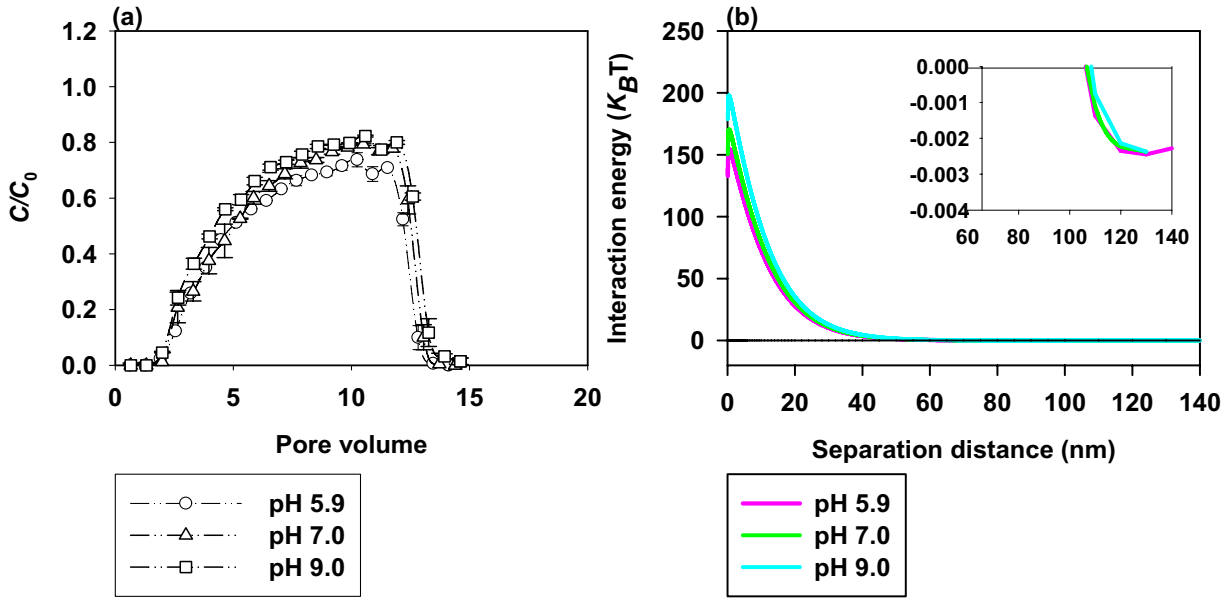

Fig. 4 Effects of various pH (5.9, 7.0, and 9.0) on the transport of PS-NPs in saturated zeolite at an ionic strength of 1 mM NaCl and a flow rate of 0.4 mL/min.: **a** breakthrough curves and **b** calculated DLVO interaction energy profiles

demonstrate an increased ability to overcome energy barriers, facilitating their deposition onto the surface of the zeolite. Additionally, compared to Ca^{2+} or Mg^{2+}, Ba^{2+} shows a stronger affinity for forming inner-sphere complexes with the oxygen-containing functional groups on the surfaces of both PS-NPs and zeolite, making it a more effective bridging agent. On the contrary, Ca^{2+} and Mg^{2+} have a tendency to create outer-sphere complexes and therefore exhibit weaker binding to solid surfaces. Analogous conclusions also have been demonstrated by Xia et al. (2017).

Effects of pH on the Transport of PS-NPs in the Saturated Zeolite

The transport of PS-NPs in the zeolite was noticeably influenced by the pH of the solution, as depicted in Fig. 4a. An increase in pH was found to enhance the PS-NPs mobility in the saturated zeolite. For example, PS-NPs were retained to a significant degree, with a $(C/C_0)_{max}$ of approximately 71.4% at the pH value of 5.9. As the pH increased, the mobility of PS-NPs increased progressively. As an example, the $(C/C_0)_{max}$ reached 79.3% and 83.2% at pH 7.0 and 9.0, respectively.

The following aspects can explain this phenomenon. The PS-NPs migration depends on the variable charges of the zeolite surface, which are pH-dependent. Considering the pH_{PZC} of zeolite, which was identified to lie around pH 6.5, the variable charges were positive at pH 5.9. In contrast, they were negative at pH 7.0 and 9.0. Therefore, at a pH of 5.9, there was a more significant electrostatic attraction between the positively charged edge sites on zeolite and the negatively charged PS-NPs. Furthermore, when the pH levels increased, the absolute values of the zeta potential for both zeolite and PS-NPs also increased. This suggests that as the pH levels rose, it became more difficult for the PS-NPs to deposit onto the zeolite. This information can be found in Table 1 and Table S1. The conclusion is also supported by the DLVO calculation results (as shown in Fig. 4b).

Conclusions

This study demonstrated the impact of zeolite on the transport of polystyrene nanoplastics (PS-NPs) under various solution chemistry conditions and flow rates. The migration of PS-NPs within zeolites was significantly influenced by factors such as flow rate, ionic strength, cation species, and pH. Notably, increased flow rates enhanced PS-NP mobility within the zeolite matrix by reducing particle-collector contact efficiency and amplifying hydrodynamic forces, which facilitated the detachment of nanoparticles from the zeolite surface. As ionic strength increased, the breakthrough capability of PS-NPs decreased, while deposition onto the zeolite surface intensified. This phenomenon was linked to changes in the interaction energies between the mineral surface and PS-NPs, with higher ionic strengths helping to overcome energy barriers and promoting adhesion to the surface. In terms of cation impact, monovalent cations exhibited a trend of $Na^+ > K^+ > Cs^+$,

while divalent cations followed $Mg^{2+} > Ca^{2+} > Ba^{2+}$. These differences were explained using DLVO theory, which considers factors such as energy barrier heights, steric hindrance, and bridging effects. Additionally, increased pH levels enhanced PS-NP mobility in the saturated zeolite, attributed to pH-dependent variable charges on the zeolite surface. Lower pH levels induced positive charges that attracted PS-NPs, while higher pH levels reduced deposition due to negative charges. These insights significantly advance our understanding of nanoplastic behavior in the natural environment.

Supplementary Information The online version contains supplementary material available at https://doi.org/10.1007/s41742-024-00698-z.

Funding This project was supported by the Postgraduate Practice Innovation Program of Jiangsu Province (SJCX24_2247) and the German Research Foundation (DFG) – Project Number 391977956 – SFB 1357.

Data Availability Supplementary Material data to this article can be found in the online version of this article.

Declarations

Conflict of Interest The authors declare that they have no known competing financial interests or personal relationships that could have appeared to influence the work reported in this paper.

Consent to Participate Not applicable.

Consent to Publication Not applicable.

Ethical Approval Not applicable.

References

Andrady A, Barnes P, Bornman J, Gouin T, Madronich S, White C, Zepp R, Jansen M (2022) Oxidation and fragmentation of plastics in a changing environment; from UV-radiation to biological degradation. Sci Total Environ 851:158022

Braun A, Klumpp E, Azzam R, Neukum C (2015) Transport and deposition of stabilized engineered silver nanoparticles in water saturated loamy sand and silty loam. Sci Total Environ 535:102–112

Cai L, Hu L, Shi H, Ye J, Zhang Y, Kim H (2018) Effects of inorganic ions and natural organic matter on the aggregation of nanoplastics. Chemosphere 197:142–151

Castan S, Henkel C, Hüffer T, Hofmann T (2021) Microplastics and nanoplastics barely enhance contaminant mobility in agricultural soils. Commun Earth Environ 2:1–9

Chen G, Li X, Wang Z, Li M, Wang W, Lu R, Wang S, Li Q, Hu Z, Wu Y, Li Z, Wang P, Cao Y (2024) Human exposure to micro(nano) plastics: health risks and analysis methods. TrAC Trends Anal Chem 178:117835

Fang B, Nakagawa K (2021) Effect of pH, ionic strength, and freezing treatment on a colloidal suspension of egg white aggregates. Food Struct Netherlands 27:100181

Fan Z, He P, Bai H, Liu J, Liu H, Liu L, Niu R, Gong J (2024) Green recycling of waste poly(ethylene terephthalate) into Ni-MOF nanorod for simultaneous interfacial solar evaporation and photocatalytic degradation of organic pollutants. EcoMat 6:e12422

Hu D, Shen M, Zhang Y, Li H, Zeng G (2019) Microplastics and nanoplastics: would they affect global biodiversity change? Environ Sci Pollut Res 26:19997–20002

Kragovic M, Dakovic A, Sekulic Z, Trgo M, Ugrina M, Peric J, Gatta GD (2012) Removal of lead from aqueous solutions by using the natural and Fe(III)-modified zeolite. Appl Surf Sci 258:3667–3673

Kumar R, Verma A, Shome A, Sinha R, Sinha S, Jha PK, Kumar R, Kumar P, Das S, Sharma P (2021) Impacts of plastic pollution on ecosystem services, sustainable development goals, and need to focus on circular economy and policy interventions. Sustainability 13:9963

Lai H, Liu X, Qu M (2022) Nanoplastics and human health: hazard identification and biointerface. Nanomaterials 12:1298

Liang Y, Bradford SA, Simunek J, Vereecken H, Klumpp E (2013) Sensitivity of the transport and retention of stabilized silver nanoparticles to physicochemical factors. Water Res 47:2572–2582

Liang T, Yang X, Liu B, Song R, Xiao F, Yang Y, Wang D, Dong M, Ren J, Xu BB, Algadi H, Yang Y (2023) Ammonium perchlorate@graphene oxide/Cu-MOF composites for efficiently catalyzing the thermal decomposition of ammonium perchlorate. Adv Compos Hybrid Mater 6:67

Lin X, Chen L, Zhong X, BaQais A, Dang W, Amin MA, Huang H, Li H, Liang G, Liu G, Yang Z (2023) N-doped bimetallic phosphides composite catalysts derived from metal-organic frameworks for electrocatalytic water splitting. Adv Compos Hybrid Mater 6:79

Liu Y, Shao H, Liu J, Cao R, Shang E, Liu S, Li Y (2021) Transport and transformation of microplastics and nanoplastics in the soil environment: a critical review. Soil Use Manag 37:224–242

Liu Y, Gu G, Lu J, Zhu L, Chen Q, Kim H, Wang J, Ji P, Cai L (2024) Decreased transport of nano- and micro-plastics in the presence of low-molecular-weight organic acids in saturated quartz sand. Sci Total Environ 921:171195

Lu T, Xia T, Qi Y, Zhang C, Chen W (2017) Effects of clay minerals on transport of graphene oxide in saturated porous media. Environ Toxicol Chem 36:655–660

Lu T, Gilfedder BS, Peng H, Niu G, Frei S (2021a) Effects of clay minerals on the transport of nanoplastics through water-saturated porous media. Sci Total Environ 796:148982

Lu T, Gilfedder BS, Peng H, Peiffer S, Papastavrou G, Ottermann K, Frei S (2021b) Relevance of iron oxyhydroxide and pore water chemistry on the mobility of nanoplastic particles in water-saturated porous media environments. Water Air Soil Pollut 232:1–13

Ma Y-B, Xie Z-Y, Hamid N, Tang Q-P, Deng J-Y, Luo L, Pei D-S (2023) Recent advances in micro (nano) plastics in the environment: distribution, health risks, challenges and future prospects. Aquat Toxicol 261:106597

Miao P, Cheng K, Li H, Gu J, Chen K, Wang S, Wang D, Liu TX, Xu BB, Kong J (2019) Poly(dimethylsilylene)diacetylene-guided ZIF-based heterostructures for full ku-band electromagnetic wave absorption. ACS Appl Mater Interfaces 11:17706–17713

Mitzel MR, Sand S, Whalen JK, Tufenkji N (2016) Hydrophobicity of biofilm coatings influences the transport dynamics of polystyrene nanoparticles in biofilm-coated sand. Water Res 92:113–120

Motsi T, Rowson N, Simmons M (2009) Adsorption of heavy metals from acid mine drainage by natural zeolite. Int J Miner Process 92:42–48

Nightingale E Jr (1959) Phenomenological theory of ion solvation. Effective radii of hydrated ions. J Phys Chem 63:1381–1387

Qiana N, Gaoa X, Lang X, Deng H, Bratu TM, Chen Q, Stapleton P, Yan B, Min W (2024) Rapid single- particle chemical imaging of nanoplastics by SRS microscopy. Proc Natl Acad Sci USA 121

Qi Z, Zhang L, Wang F, Hou L, Chen W (2014) Factors controlling transport of graphene oxide nanoparticles in saturated sand columns. Environ Toxicol Chem 33:998–1004

Quevedo IR, Tufenkji N (2012) Mobility of functionalized quantum dots and a model polystyrene nanoparticle in saturated quartz sand and loamy sand. Environ Sci Technol 46:4449–4457

Qu M, Miao L, Liu X, Lai H, Hao D, Zhang X, Chen H, Li H (2023) Organismal response to micro(nano)plastics at environmentally relevant concentrations: toxicity and the underlying mechanisms. Ecotoxicol Environ Saf 254:114745

Rahman A, Sarkar A, Yadav OP, Achari G, Slobodnik J (2021) Potential human health risks due to environmental exposure to nano-and microplastics and knowledge gaps: a scoping review. Sci Total Environ 757:143872

Sasidharan S, Torkzaban S, Bradford SA, Dillon PJ, Cook PG (2014) Coupled effects of hydrodynamic and solution chemistry on long-term nanoparticle transport and deposition in saturated porous media. Colloids Surf A Physicochem Eng Asp 457:169–179

Shang X, Mei H, Li Z, Dong C, Wang Z, Xu B (2021) Improved ionic diffusion and interfacial charge/mass transfer of ZIF-67-derived Ni-Co-LDH electrodes with bare ZIF-residual for enhanced supercapacitor performance. New J Chem 45:13979–13985

Sharma P, Bao D, Fagerlund F (2014) Deposition and mobilization of functionalized multiwall carbon nanotubes in saturated porous media: effect of grain size, flow velocity and solution chemistry. Environ Earth Sci 72:3025–3035

Sharma MD, Elanjickal AI, Mankar JS, Krupadam RJ (2020) Assessment of cancer risk of microplastics enriched with polycyclic aromatic hydrocarbons. J Hazard Mater 398:122994

Shen M, Zhang Y, Zhu Y, Song B, Zeng G, Hu D, Wen X, Ren X (2019) Recent advances in toxicological research of nanoplastics in the environment: a review. Environ Pollut 252:511–521

Shu Y, Zhao Y, Linghu X, Liu W, Shan D, Zhang C, Yi R, Li X, Wang B (2024) $NaGdF_4$:Yb, Er@ZIF-8/MnO_2 for photocatalytic removal of organic pollutants and pathogenic bacteria. EcoMat 6:e12427

Sowunmi AR, Folayan CO, Anafi FO, Ajayi OA, Omisanya NO, Obada DO, Dodoo-Arhin D (2018) Dataset on the comparison of synthesized and commercial zeolites for potential solar adsorption refrigerating system. Data Brief 20:90–95

Szala B, Bajda T, Jelen A (2015) Removal of chromium (VI) from aqueous solutions using zeolites modified with HDTMA and ODTMA surfactants. Clay Miner 50:103–115

Sze A, Erickson D, Ren L, Li D (2003) Zeta-potential measurement using the Smoluchowski equation and the slope of the current–time relationship in electroosmotic flow. J Colloid Interface Sci 261:402–410

Tsitsishvili GV, Skhirtladze NS, Andronikashvili TG, Tsitsishvili VG, Dolidze AV (1999) Natural zeolites of Georgia: occurrences, properties, and application. In: Kiricsi I, PalBorbely G, Nagy JB, Karge HG, (eds) Porous materials in environmentally friendly processes, pp 715–722

Wang D-S, Mukhtar A, Wu K-M, Gu L, Cao X (2019) Multi-segmented nanowires: a high tech bright future. Materials 12:3908

Wang D, Mukhtar A, Humayun M, Wu K, Du Z, Wang S, Zhang Y (2022) A critical review on nanowire-motors: design. Mech Appl Chem Rec 22:e202200016

Wang M, Gao B, Tang D (2016) Review of key factors controlling engineered nanoparticle transport in porous media. J Hazard Mater 318:233–246

Wu X, Lyu X, Li Z, Gao B, Zeng X, Wu J, Sun Y (2020) Transport of polystyrene nanoplastics in natural soils: effect of soil properties, ionic strength and cation type. Sci Total Environ 707:136065

Xia T, Fortner JD, Zhu D, Qi Z, Chen W (2015) Transport of sulfide-reduced graphene oxide in saturated quartz sand: cation-dependent retention mechanisms. Environ Sci Technol 49:11468–11475

Xia T, Qi Y, Liu J, Qi Z, Chen W, Wiesner MR (2017) Cation-inhibited transport of graphene oxide nanomaterials in saturated porous media: the Hofmeister effects. Environ Sci Technol 51:828–837

Yu Y, Flury M (2021) Current understanding of subsurface transport of micro- and nanoplastics in soil. Vadose Zone J 20:e20108

Yu T, Huang X, Zhang XF, Li K, Liu SP, Dai N, Zhang K, Zhang YX, Li H (2024) A review of nanomaterials with excellent purification potential for the removal of micro- and nanoplastics from liquid. DeCarbon 5:100064

Zhang M, Hou J, Wu J, Miao L, Zeng Y (2023a) Effects of input concentration, media particle size, and flow rate on fate of polystyrene nanoplastics in saturated porous media. Sci Total Environ 881:163237

Zhang M, Hou J, Xia J, Zeng Y, Miao L (2023b) Influences of input concentration, media particle size, metal cation valence, and ionic concentration on the transport, long-term release, and particle breakage of polyvinyl chloride nanoplastics in saturated porous mediae. Chemosphere 322:138130

Zhang M, Yang S, Zhong W, Wang H, Uthappa UT, Wang B (2024) Upscaling waste human hairs into micro/nanorobots for adsorptive removal of micro/nanoplastics. Chem Eng J 495:153264